# Stellar Encounters at the Galactic Centre

*Robert Fisers*

Lund Observatory
Lund University

2022-EXA187

Degree project of 15 higher education credits
January 2022

Supervisor: Ross Church

Lund Observatory
Box 43
SE-221 00  Lund
Sweden

# Contents

# Abstract

Using methods of smoothed particle hydrodynamics (SPH) an $N$-body simulation was set-up to investigate stellar encounters between a 1 $M_{\odot}$ main sequence (MS) star, modeled after the Sun, and a 0.6 $M_{\odot}$ white dwarf (WD). This was done primarily to investigate the assumptions made by Mastrobuono-Battisti et al. (2021) in search of the impact of stellar encounters on stellar population in nuclear stellar clusters (NSCs). Four different possible outcomes of the encounter were identified and described in detail. The boundary between a merger taking place between the stars and no merger was located in velocity-periastron space. Properties, such as, change in specific orbital energy and mass of the WD were investigated for a set of select encounters sharing the same velocity of the WD to look for relations between different input parameters of the encounter. It was found that the assumptions about no mass loss and the location of the boundary of the merger and no-merger encounters between WDs and MS stars made by Mastrobuono-Battisti et al. (2021) were false. I show that in encounters, where either a physical collision or a merger between the two stars takes place, a substantial amount of unbound mass is produced, and that encounters with periastron values larger than 1.0 $R_{\odot}$ can result in a merger, given that the kinetic energy of the WD is sufficiently small. The possible effects of these findings on the evolution of stellar population in NSCs were discussed. Less significant relations between the mass accreted by the WD, WDs final velocity, orbital period of the WD in lengthy merger encounters and periastron value of the encounter were also analysed and summarized.

# Popular science article

Imagine a rogue star was on a collision path to cross through the Solar System. What are the possible outcomes of this meeting, and what parameters decide the severity of it? How would our Sun change, and how would its future be effected? These are some of the major questions the study of stellar encounters tries to answer. In this article I will sketch short answers to the above questions and sum up the study of stellar encounters, with focus on encounters between main sequence stars like the Sun and some of the oldest stars in the Universe - white dwarfs.

In most places in the Universe one should not be concerned about such an event taking place, as distances between star orbits are so large that the probability that they cross each others gravitational pull is very, very small. However, in the densest regions in the Universe, termed nuclear star clusters, the orbits are so closely packed that such events are a common occurrence. The best place for us to study these encounters is the centre of our own Milky Way galaxy. Despite the galactic centre being the closest nuclear star cluster to us, physical observations are still hard to perform, mostly due to two reasons: firstly, the galactic centre is majorly populated by many bright stars and dust making visual observations very hard to perform; secondly since we are studying astronomical events, the time scale accordingly is not suited for human observations. To by pass these problems, we invoke methods of computational physics by performing advanced computer simulations based on hydrodynamics models used to simulate, for example, a ball moving in a water tank.

Stellar encounters come in different verities, depending on the stars that are meeting. For each type of encounter the final result and the impact of the encounter on the stellar population in nuclear star cluster will depend on the type of stars involved. For encounters between Sun like stars and white dwarfs the final result can either be a merger between the two stars, or the white dwarf escaping the gravitational pull of the main sequence star. The outcome and the severity of it, in broad strokes, mainly depends on the rate at which the distance between the stars decreases and the distance of the closest approach between them. These two parameters will decide if the product of the encounter will be a star still capable of nuclear fusion in its core, a dim object destined to remain faint for the rest of its existence, or two separate objects which have undergone a traumatizing experience and must carry on with their lives to best of their abilities. In either of the outcomes, a lasting impact is left on the products of the encounter. In most cases the structure of the star is heavily altered, in some even irreversibly. This experience alters the future evolution of the star, disrupting it from its normal evolutionary path. Given a number of these encounters can take place in the nuclear star clusters, the normal evolutionary path of the star cluster could be altered.

In summary, a star passing so close to the Sun that it might alter its future is not something we should worry about. However, the study of stellar encounters allows us to better understand the evolution of stars exposed to such events, how their internal structure has changed, what parameters decide the severity of encounter and what relationships exist between them, and how big of a role in evolution of the stellar population in nuclear star clusters do stellar encounters play.

# 1 Introduction

In order to observe and investigate stellar encounters one must seek some of the densest regions in the Universe, as elsewhere the encounter probability is very very small. Nuclear star clusters (NSCs), being some of the densest stellar systems in the Universe are a prime location to carry out such investigation, and are found at the centres of large galaxies. Our own Milky Way galaxy hosts such a NSC around its $4.3 \cdot 10^6$ $M_\odot$ super massive black hole (SMBH) Sagittarius A* (Gillessen et al. 2017). The NSC of Milky Way has been estimated to have total mass of $2.5 \cdot 10^7$ $M_\odot$ and projected half-light radius of 4.2 pc (Schödel, R. et al. 2014). About 80 % of the total mass formed 10 Gyr ago, while the remainder is from more recent star formation episodes taking place 5 Gyr ago and 100 Myr ago (Schödel, R. et al. 2020).

The larger purpose of this project is to investigate what impact on stellar population of observable giants in NSCs stellar encounters have. Mastrobuono-Battisti et al. (2021) concluded that the overall impact of stellar encounters on the stellar population of observable giants in the NSC they built was minor. That is, the change in the number of observable giants in the NSC did not experience any large increase or decrease outside of the standard evolution of a star cluster, which could be attributed to stellar encounters taking place. An $N$-body simulation was used to model a Milky Way-like NSC formed through a merger of massive stellar clusters. However, it was acknowledged that the result might change if the model was built differently. As some of the explanations for the low impact of encounters on the population distribution the authors mentioned three of the following reasons: firstly, the $N$-body model used instead of forming a cusp formed a core, which in turn limited the central number density and consequently the collision rate; secondly, the rate of stellar encounters was minimized due to the presence of the SMBH from the start of the simulation, which caused high velocity dispersion; thirdly, the two outcomes of main sequence - main sequence (MS-MS) encounters equaled out. That is, the MS-MS encounter results in a merger, which accelerates the evolution of the formed star. For more massive MS stars this leads to the star evolving past the giant phase at a much faster rate, while the lower mass MS stars evolve to the giant phase faster. Hence, the overall population of observable giants remains relatively unaffected. On top of this, several smaller assumptions were made, such as, constant white dwarf mass (WD), no mass loss during merger encounters between two MS stars, and a MS star and a WD, and that the outcome of MS-MS and MS-WD encounters is independent of impactor velocity and results in a merger only when physical collision between the two stars takes place during the first passage of the impactor. Due to these reasons, the authors suggested using Monte Carlo simulations (e.g. Giersz et al. 2013) to build more realistic models, and models containing a steeper NSC density profile. Another option, which is why this project is contributing to this research, is to look at the different kinds of collisions separately to understand their underlying principles and possible implications on the stellar population in more detail.

In this project, stellar encounters between a MS star and a WD will be studied by varying the initial kinetic energy and periastron value of the WD to investigate if the assumptions made by Mastrobuono-Battisti et al. (2021) are in fact accurate. An attempt to locate the boundary between merger and no-merger encounters in velocity-periastron space will be

made. The change in mass distribution in the system, the structure of the MS star due to experiencing an encounter with a WD, and the change in kinetic energy of the WD due to encountering a MS star will be investigated for both individual encounters and encounters sharing the same intial velocity of the WD. As well as contributing to the research of Mastrobuono-Battisti et al. (2021) on the impact of stellar encounters on evolution of stellar population in NSCs, this project can serve as guidance in research of stellar encounter products and evolution of stars involved in stellar encounters. While only encounters between MS stars and WDs are studied, some of the presented results and techniques can be carried over as guidelines for expected results to other types of encounters, for example, encounters between two MS stars, or between MS star and a giant.

# 2 Method

## 2.1 SPH Code

Smoothed Particle Hydrodynamics (SPH) is a computational technique used to model hydrodynamical flows in a fast and efficient manner. SPH stands apart from other hydrodynamical techniques by the fact that it is able to bypass the need for a grid to compute derivatives, which in turn avoids possible problems, such as, distortion and mesh tangling. On top of this, SPH is based on Lagrangian formulation which allows for easy implementation of $N$-dimensions and is well suited for astrophysical problems. Past developments in hierarchical tree methods (Appel, A. W. 1985; Jernigan, J. G. 1985; Barnes, J. & Hut, P. 1986) designed for calculating gravitational forces in an $N$-body simulations, set a basis for fast and effective calculations of gravitational forces with easy way of varying the SPH analog of an adaptive grid - the smoothing length. The efficiency of SPH is almost solely determined by how fast the code is able to locate nearby particles in a given radius(smoothing length) around a given particle. In this section I present the basis on which SPH is built such that all important conservation laws are satisfied, how the smoothing length is introduced, and different approaches used to implement the time step.

SPH functions by dividing a fluid into a set of discrete moving elements $i, j$ called particles which interact via the kernel function $W$. An arbitrary function in SPH is defined as

$$\langle f(\vec{r})\rangle = \int W(\vec{r}-\vec{r'},h)f(\vec{r'})d\vec{r'}, \tag{1}$$

where the kernel function $W$ is normalized as

$$\int W(\vec{r},h)d\vec{r} = 1,$$

and $h$ is the variable smoothing length defining the characteristic radius of the kernel function. This definition alone is enough to already introduce particles with positions and mass in SPH. For example, starting from Equation 1 and using Taylor expansion around $\vec{r}=\vec{r'}$, limiting $W$ to only even functions, and introducing particle distribution according to number density distribution, one can find the expression for fluid density as

$$\langle \rho(\vec{r})\rangle = \sum_{j=1}^{N} m_j W(|\vec{r}-\vec{r'}|,h). \tag{2}$$

As with any physical computational methods, certain conservation laws have to be satisfied. These conservation laws introduce limitations to the otherwise seemingly completely free choice of the kernel function $W$, but explaining full derivations of them is beyond the scope of this section. Therefore, only most important conservation laws and stand alone versions of their equations in SPH formalism derived by Benz, W. (1986) are presented.

Two of the arguably most important conservation laws in physics are the conservation of momentum and energy. For astrophysical problems where the fluid is contained by its self-gravity the conservation of momentum in SPH formalism is defined as

$$\frac{d\vec{v}_i}{dt} = -\sum_{j=i}^{N} m_j \left( \frac{P_i}{\rho_i^2} + \frac{P_j}{\rho_j^2} \right) \vec{\nabla}_i W(|\vec{r}_i - \vec{r}_j|, h), \tag{3}$$

where $P_i$ is the pressure exerted on particle $i$, $v_i$ is the velocity of particle $i$, and $\rho_i$ is the density of particle $i$. While conservation of energy in SPH is defined as

$$\frac{du_i}{dt} = \frac{P_i}{\rho_i^2} \sum_{j=1}^{N} m_j (\vec{v}_i - \vec{v}_j) \vec{\nabla} W(|\vec{r}_i - \vec{r}_j|, h), \tag{4}$$

where $u_i$ represents the specific internal energy of particle $i$.

Modifications to the above conservation laws are introduced when introducing viscosity, radiation transport and self-gravity to the SPH. Since radiation transport is not of interest for this project, it will not be mentioned further. For viscosity most commonly bulk viscosity

$$\Pi_l = -\alpha \rho l c_s \vec{\nabla} \cdot \vec{v}$$

or von Neumann - Richtmyer

$$\Pi_q = \beta \rho l^2 (\vec{\nabla} \cdot \vec{v})^2$$

definitions of artificial viscous pressure term $\Pi_{ij}$ are introduced on the right hand side of the momentum Equation 3 and the specific internal energy Equation 4. In the above equations $\alpha$ and $\beta$ are free variables, $l$ is the length scale over which the shock is spread, $c_s$ the speed of sound in the medium. When considering self-gravity of particles, infinite mass needs to be avoided. Thus, the following constraint on the kernel is introduced:

$$\int_0^\infty r^2 W(r, h) dr < \infty.$$

The total gravitational force $\vec{\nabla}\phi_i$ felt by particle $i$ can be expressed as a sum of individual forces

$$-\vec{\nabla}\phi_i = -G \sum_{j=i}^{N} \frac{M(|\vec{r}_i - \vec{r}_j|)}{|\vec{r}_i - \vec{r}_j|^2} \frac{(\vec{r}_i - \vec{r}_j)}{|\vec{r}_i - \vec{r}_j|}. \tag{5}$$

Since the above summation scales with the number of particles squared, hierarchical tree methods are implemented, which locate all neighbouring particles in a fast manner and scale

the self gravity as $Nlog(N)$ instead, significantly improving the computational time for many particle simulations and retaining the desired accuracy.

All of the above expressions were derived assuming a constant smoothing length $h$. When working with gravitational systems this used to be the preferred approach as variable smoothing length can cause issues with potential energy and, therefore, energy conservation. However, for cases where one wishes to obtain optimal resolution of the fluid a variable smoothing length is assigned to each particle depending on its local conditions. In this way, in more dense regions a shorter smoothing length is used to better resolve and more efficiently calculate forces on each particle, while in lower density regions a longer smoothing length is used. Although the scale over which $h$ varies can not significantly exceed $h$ itself. This is because introducing a variable smoothing length requires the introduction of more new terms to the above conservation laws and definitions of self-gravity and viscosity, which, if $h$ varies over a large range of values, become extremely complicated to calculate. Despite this, a variable smoothing length can increase the computational speed in many particle systems where not all particles experience change in forces at the same time.

Along the way to deriving momentum and energy conservation laws and introducing viscosity and self-gravity to SPH many constraints to the kernel function $W$ were introduced. On top of this, the choice of the shape of the kernel function is of importance to avoid the formation of artificial clumps of particles. Three of the most common kernel functions satisfying all of the necessary conditions are: exponential kernel (Wood D. 1981), Gaussian (Gingold, R. A. & Monaghan JJ. 1977), and Spline (Monaghan, JJ. & Mattanzio, J. C. 1985), which the SPH code used for this project used:

$$W(r,h) = \frac{1}{\pi h^3} \begin{cases} 1 - \frac{3}{2}\nu^2 + \frac{3}{4}\nu^3, \text{ if } 0 \leq \nu \leq 1; \\ \frac{1}{4}(2-\nu)^3, \text{ if } 1 \leq \nu \leq 2; \\ 0, \text{ otherwise,} \end{cases}$$

where $\nu = \frac{r}{h}$. All of the above kernels interpolate to the second order of $h$. It is possible to formulate kernels which interpolate to higher orders of $h$, but precaution has to be taken to avoid negative values and still satisfy all of the constraints. Deriving such kernels is beyond the scope of this section.

The introduction of time in SPH does not differ from other methods. Standard leap-frog or predictor-corrector methods are most commonly used, but methods involving individual time steps for each of the particles built on hierarchy of time steps based on powers of 2 are preferred in $N$-body simulations. Use of altering time step can has also be seen in practice, where the length of the time step changes depending on the change in forces on particles, for example, when a large shock wave is induced the time step would be shortened. On top of this, it is also possible to combine different time step methods and let the code choose the most efficient and accurate one during each period of the simulation.

## 2.2 Setting up the system

To begin simulating different encounters between a MS star and the WD the stars themselves needed to be introduced. This began by creating the MS star using parameters of the Sun and 40 000 particles. Which involved solving equations of stellar structure and evolution (Eggleton, P. P. 1971; Pols et al. 1995) using the STARS code, with input parameters being those of the Sun. When the model was built, it initially was not in equilibrium due to the code discretising the input into a set of particles, which caused the forces felt by different particles to initially be different from their actual value as the average value over the spherical shell was assigned to each particle. In order to relax the system, and prevent the star from collapsing in on itself or expanding, dampening, a force to counteract forces in the system and accelerate the rate at which equilibrium is reached, was introduced. Different values of dampening were tested by observing the MS star over 16.8 dynamical time scales, time corresponding to the time it would take for a particle to free-fall to the centre of the MS star and 20 large time steps in the simulation. It was looked for no visual distortions in the structure of the MS star, while reaching the equilibrium in a reasonable time scale, that is, before 16.8 dynamical time scales had passed. The final value of dampening of 10 $[\frac{GM_\odot}{R_\odot^2}]$ was chosen.

Afterwards the encounter could be set-up. This was done using an executable called starcollider, where the parameters of the WD such as velocity at infinity $v_{inf}$, periastron $d_{min}$, initial separation $r$ were inserted along side the file containing the model MS star. A graphical representation of the system can be seen in Figure 1.

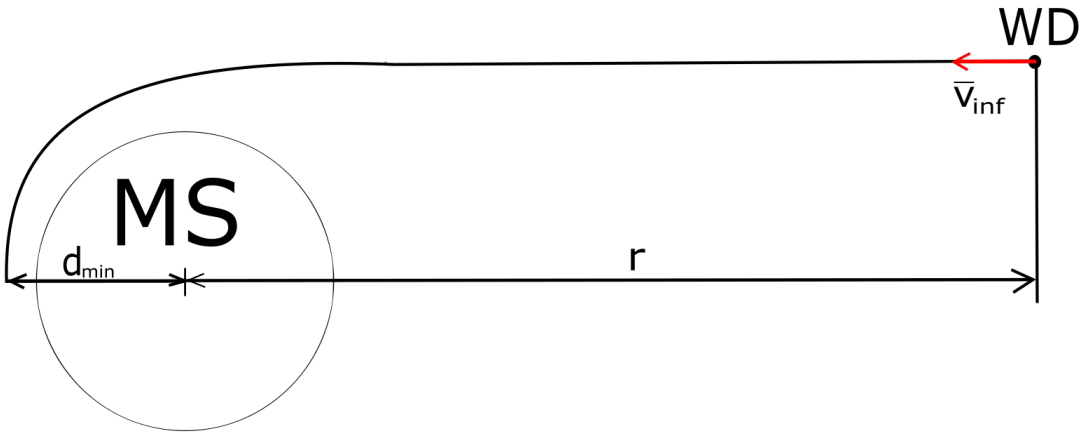


Figure 1: A sketch of the system of an encounter between a white dwarf and a main sequence star at the initial state.

From here using the SPH code written by Benz the simulation was carried out by executing the hierarchical tree executable, which solved the equations mentioned in the previous section with small time step of 0.0125 dynamical time scales, and large time step of 0.8 dynamical time scales.

In order to understand the results produced one has to understand in what units all of the calculations and simulation were carried out. For this task Solar units were used. That is $R = 1.0$ corresponds to 1.0 $R_\odot$, $M = 1.0$ to 1.0 $M_\odot$, $G = 1$, and, therefore,

$v_{inf} = 1.0\ \sqrt{GM_\odot/R_\odot}$ to approximately 436 $km/s$, while a single time unit corresponds to a single dynamical time scale of the MS star.

## 2.3 Analysis code

To investigate the outcome of the encounter a python code, which searches for sets of mutually bound particles, was made. This was done by defining a function which, when looped through all of the simulation output files, performed the following. First the text output files of the simulation were read in. These files contained information regarding position, velocity, mass and density of each particle contained in the system at the chosen time step of the simulation.

Then the exact position and velocity of each Cartesian component of the particles originally composing the MS star in the centre of mass frame was calculated using the following relations:

$$M = \sum_i^n m_i, \tag{6}$$

$$X = \frac{\sum_i^n m_i x_i}{M}, \tag{7}$$

$$V = \frac{\sum_i^n m_i v_{x,i}}{M}, \tag{8}$$

where $n$ stands for the total amount of particles present in the simulation minus the point mass WD. Equations 7 and 8 display the calculation only for the x-component, but were also done for y and z components. The obtained values were combined to give the position and velocity in vector notation with respect to the center of mass of the particles originally composing the MS star. This was done by subtracting the corresponding centre of mass values from the calculated values. For the point mass these values were directly obtained from the output file of the simulation.

Afterwards for each of the particles involved in the encounter the specific energy $\epsilon$ with respect to the centre of the mass of the particles originally composing the MS star for the MS star and the point mass WD were calculated using

$$\epsilon_{i,*} = \frac{1}{2}|\vec{v}_i - \vec{v}_*|^2 - \frac{GM_*}{|\vec{r}_i - \vec{r}_*|}, \tag{9}$$

$$\epsilon_{i,PM} = \frac{1}{2}|\vec{v}_i - \vec{v}_{PM}|^2 - \frac{GM_*}{|\vec{r}_i - \vec{r}_{PM}|}. \tag{10}$$

Using these specific energies $\epsilon$ it was possible to characterize and count where each of the particles belonged at the specific time step of the simulation. If $\epsilon_{i,*} > 0$ and $\epsilon_{i,PM} > 0$ the particle was unbound, and did not belong to either the MS star nor the WD. If the above statement was not true, then the particle belonged to either the MS star or the point mass, which was deducted by checking if the condition $\epsilon_{i,*} < \epsilon_{i,PM}$ was true. If it was, then the particle belonged to the MS star. If not, then the particle belonged to the WD.

Where each of the particles belonged was counted, and the code was set to loop through the sorting process until the obtained mass of each for the bodies was the same as in the

previous iteration. On top of this, the specific orbital energy $\epsilon$ of the WD around the MS star was calculated using the relation:

$$\epsilon = \frac{1}{2}|\vec{v}_* - \vec{v}_{PM}|^2 - \frac{G(M_* + M_{PM})}{|\vec{r}_* - \vec{r}_{PM}|}. \tag{11}$$

This was done for each iteration in the loop, but only final value representing the converged result was saved. The above specific energy relations, Equations 9, 10 and 11, the potential energy term is exact only when working with spherical symmetry. That is, as the MS star is disrupted by the WD, the spherical symmetry is lost to a degree depending on the impact parameters, and the potential energy can only be treated as an approximation. Despite this, the consequences of using this approximation on the final result should not be substantial for most of the cases investigated. The majority of the MS stars mass resides in its core which in the majority of encounters should not experience substantial deformation. Additionally, the evolution of the merged object or the remnant MS star after the encounter tends towards the equilibrium configuration, which implies spherical shape.

When it was identified where each of the particles belong, the properties of these particles were written out on three different output files, one for each of: composing MS star, bound to the WD, and unbound. These files were later on used in further analysis discussed in following sections. The python code can be found in Appendix A.

## 2.4 Analysis of the encounters

### 2.4.1 Individual encounters

Qualitative inspection of the simulated encounters revealed three major types of encounters: destruction of the MS star, merger between the MS star and the WD, which had two distinct ways of occurring, and no-merger, where the WD escapes the gravitational pull of the MS star. For this purpose, figures displaying the density of the MS star or the merged object, depending on the encounter type, as a function of distance from the centre of the star were made.

To aid the understanding of the processes that have lead to the obtained density distributions the mass change of the bodies in the system as a function of time was plotted. These figures provided an insight of the rate at which the WD accreted the mass of the MS star during the encounter, exactly when the merger between the two stars took place, and how the unbound mass behaved after the encounter. To further the understanding of the encounter, and to identify similarities and differences between the different encounter types, figures displaying the specific orbital energy $\epsilon$ as a function of time were produced. These figures allowed to clearly identify between two different kinds of merger encounters, and provided an insight in what happens with the WD and the MS star during the merger encounter. When the merger has taken place the specific orbital energy $\epsilon$ according to Equation 11 is not defined. Therefore, for illustration purposes when an undefined energy value was obtained it was set to be 0.

### 2.4.2 Grid of encounters

After investigating different kinds of possible encounters individually and making comparisons between each of the cases, the whole population of performed encounters was looked at. Primary focus was to determine where the boundary between WD being captured by the MS star and merging with it, and escaping the gravity of the MS star lies, and whether there are relations between these input parameters, which could be used to determine the outcome of the encounter without performing the simulation. These results would allow to estimate the number of merger encounters taking place for a given velocity dispersion. For this purpose a figure displaying all of the performed encounters on a $d_{min}$ vs $v_{inf}$ grid was made, and the encounters were categorized based on their outcome. In addition, for a set of simulated encounters with the same WD velocity at infinity $v_{inf}$ the difference between the initial and final mass of the unbound mass, mass of the MS star and the mass accreted by the WD was plotted. Similarly the difference in specific orbital energy $\epsilon$ was plotted. This was done in order to look for relations which would allow one to estimate these values for a certain encounter without performing it, to look for relations between different $v_{inf}$ values, or determine the outcome of the encounter if present only by these values. The orbital period $T$ of the WD for encounters resulting in a merger, located on the boundary between a merger and no-merger was also investigated to gain an understanding on the time scale these encounters take place and how far from the actual boundary the obtained result for the corresponding $d_{min}$ and $v_{inf}$ values is.

# 3 Results and analysis

## 3.1 Individual collisions

Individual encounters between a 0.6 $M_\odot$ WD and a 1.0 $M_\odot$, 1.0 $R_\odot$ MS star modeled after the Sun with initial separation $r = 5.0$ $R_\odot$ between the centre of mass of the MS star and the WD were investigated first, see Figure 1. The possible outcomes of these encounters can be categorized in four different cases: direct capture of the WD where no prominent orbital motion before the merger is observed and WD does not maintain enough kinetic energy to exit the MS star; merger via orbital motion of the WD, where the WD merges with the MS star through undergoing orbital motion around the centre of mass of the MS star; no capture of the WD; destruction of the MS star. For each of these cases four different figures were investigated: illustration of the MS star after the encounter; density $\rho$ distribution of the merged object or the remaining MS star, distribution of the total mass during the encounter; and specific orbital energy $\epsilon$ between the MS star and WD during the encounter. Figure 2 shows particles composing the MS star before the encounter for reference purposes.

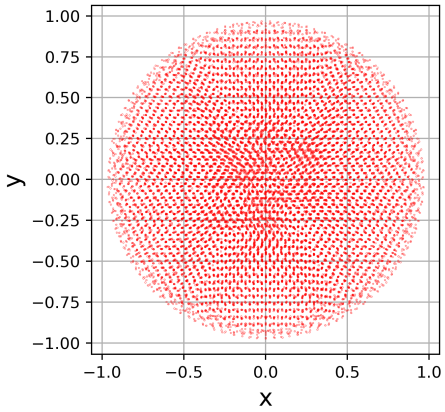


Figure 2: Figure displaying the particles composing the MS star in xy-plane at a relaxed state before the encounter with a WD.

### 3.1.1 Destruction of the main sequence star

Destruction of the MS star occurs in cases when the periastron value $d_{min}$ is small, and the relative velocity at infinity $v_{inf}$ is very large, leaving the MS star in a very disturbed state, and the WD escaping the gravity of the remnants of the MS star. These types of encounters are very rare, as the required range of periastron values for this type of encounter to occur is very small, almost head on collisions, and not commonly encountered. On top of this, the required $v_{inf}$ values are not encountered in most velocity dispersions.

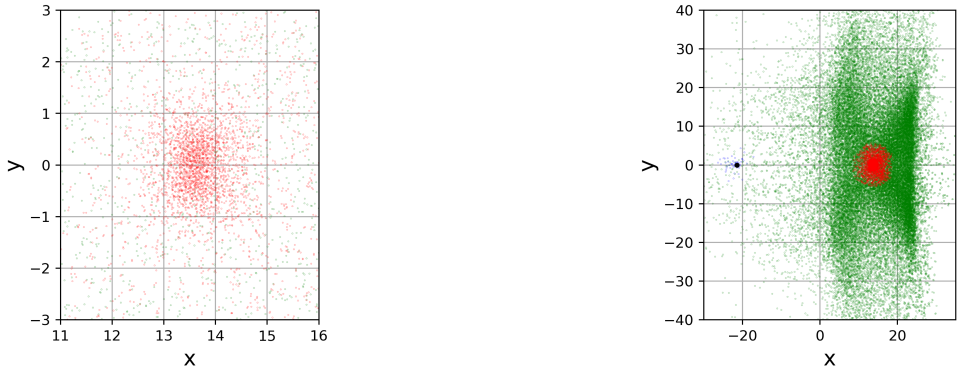


(a) (b)

Figure 3: Illustrations of the remnants of the MS star after encounter with a WD with $v_{inf} = 5.0$ and periastron $d_{min} = 0.0$. Snapshot taken 8.7 dynamical time scales into the simulation. The red dots indicate the particles composing the star, green are unbound, and blue accreted by the WD. (a) Displays zoomed in look at the remnants of the MS star from Figure (b).

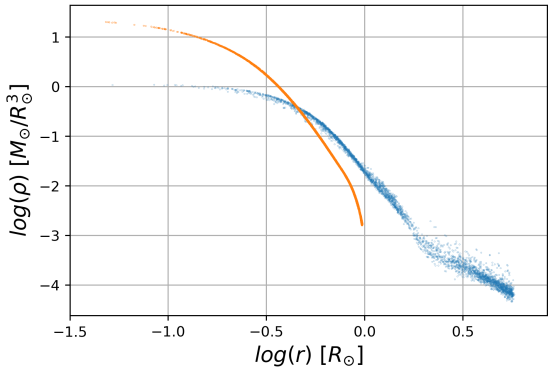


Figure 4: Density distribution of the remnant of the MS star as a function of distance in an encounter with a WD with $v_{inf} = 5.0$ and periastron $d_{min} = 0.0$. Orange points represent the initial density distribution, and blue points represent the density distribution 8.7 dynamical time scales into the encounter.

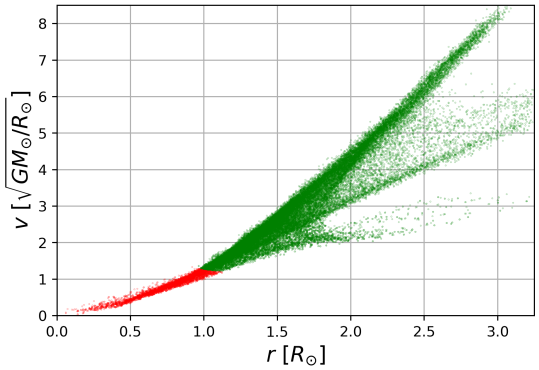


Figure 5: Velocity of the particles composing the MS star (red), and unbound (green) 1.7 dynamical time scales into the simulation, that is, shortly after the collision between the WD and MS star, when the velocity of the particles is the largest in a destruction encounter.

Figure 3*b* displays an extreme velocity case of a head on collision between a 0.6 $M_\odot$ WD with $v_{inf} = 5.0$, $d_{min} = 0.0$ and a 1.0 $M_\odot$ MS star 8.7 dynamical time scales into the simulation, where the WD pierces through the star like a bullet. The expected result of this type of encounter was that the MS star would be completely destroyed and all of its mass became unbound matter. Contrary to this, the obtained result in Figures 3 shows that a noticeable part of the MS star has remained bound. This can be explained by the fact that the particles in the core and around it had not gained enough momentum to separate far enough from each other and escape the potential well, as well as lost a large fraction of their initial kinetic energy through collisions with other particles. That is, they did not obtain the necessary escape velocity. The distribution of particle velocities as a function of distance from the centre of the MS star shortly after the collision with the WD has taken place, that is, when the distribution is at maximum, can be seen in Figure 5. As it can be seen the unbound particles have velocities greater than the escape velocity of the Sun, approximately $v = 1.5$ in the units used, but all the particles that remained bound have velocities less than the escape velocity. The major reason as to why these particles have lower velocities is that these particles were located in the inner regions of the MS star, and lost their initial momentum through numbers of collisions with other particles. The final shape and further evolution of the remnant star is not clear and beyond the scope of this project, but one can expect that the particles which remained bound will slowly lose their velocities and fall back towards the remainder of the MS star, resulting in more compact object than illustrated in Figure 3*a*.

Figure 4 shows the density distribution of the particles forming the remnants of the MS star 8.7 dynamical time scales into the simulation. Due to the large deposit of kinetic energy from the WD, a large amount of particles have been dislocated from their original positions from the momentum gained via the induced shock wave, and the envelope of this body extends beyond 5 $R_\odot$, but is expected to shrink over time. Since the WD passed through

the very core of the star and carried a lot of momentum the density in this region has notably decreased, and the particles originally composing the core have been dislocated to other regions of the star, as can be seen from density increasing from the initial distribution starting from approximately 0.5 $R_\odot$.

The distribution of total mass of the system during the encounter can be seen in Figure 6. The WD did not accrete any noticeable mass due to its very short interaction time with the MS star. The amount of unbound mass increased steadily during the passage of the WD through the star and increased slightly afterwards as more particles with high momentum from the inner regions of the MS star deposited this energy in middle and outer region particles. After the encounter the total mass of the remnants of the MS star settled at about 0.75 $M_\odot$. The aforementioned expected total destruction of the MS star would have had a sharp decrease of the MS stars mass, all of which would have became unbound mass.

In Figure 7 one can see how the specific orbital energy $\epsilon$ according to Equation 11 changed during the duration of the encounter. As the WD collides with the MS star, a large portion of its kinetic energy is lost and deposited in the particles composing the MS star. However, as the remaining kinetic energy is still larger than the gravitational potential energy of the remnants of the MS star, the WD escapes the gravitational potential. Increase in energy after the initial deposition of kinetic energy is due to the potential term decreasing as the WD distances itself from the remnant of the MS star asymptotically tending towards approximately $\epsilon = 9.5$ as the distance between the objects keeps increasing, indicating that the final velocity of the WD is a little less than $\frac{4}{5}$ of the initial velocity.

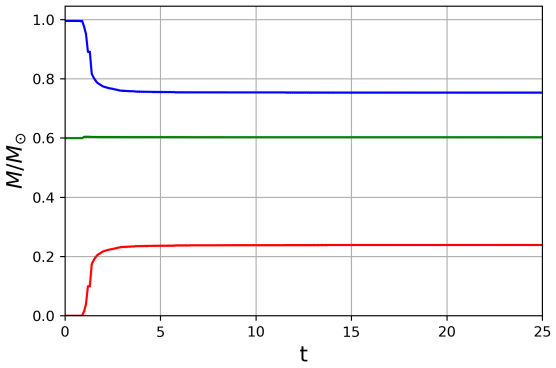


Figure 6: Mass as a function of dynamical time scales in an encounter between MS star and a WD with $v_{inf} = 5.0$ and periastron value $d_{min} = 0.0$. Blue line displays the mass of the MS star, green that of the WD, and red the unbound mass.

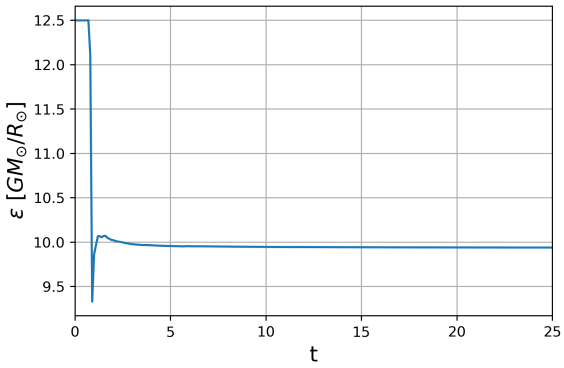


Figure 7: Specific orbital energy $\epsilon$ of the system during the encounter between MS star and a WD with $v_{inf} = 5.0$ and periastron value $d_{min} = 0.0$ as a function of dynamical time scales.

### 3.1.2 Direct capture

Direct capture of the WD mainly occurs when the periastron value is small and $v_{inf}$ is not large enough to carry the WD through all of the MS star. This is mainly due to high density of matter in the inner regions of the MS star, and that the path to travel through the star for small $d_{min}$ values is longer. However, direct merger scenario can also be observed for larger $d_{min}$ values, in compensation requiring very small $v_{inf}$ values. These conditions lead to an almost immediate merger between the stars, without any distinct orbital motion around the centre of mass of the two bodies.

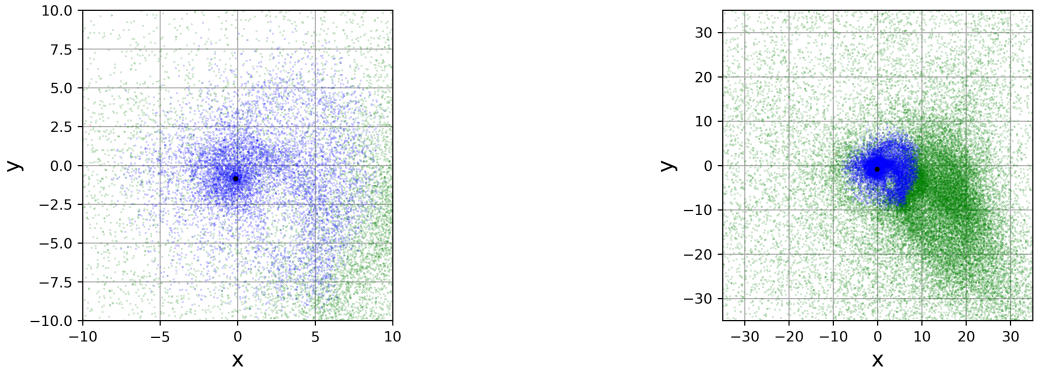


(a) (b)

Figure 8: Illustrations of the merged object after an encounter between MS star and a WD with $v_{inf} = 1.3$ and periastron $d_{min} = 0.15$. Snapshot taken 16.7 dynamical time scales into the simulation. The blue dots indicate the particles composing the merged object and green are unbound. (a) displays zoomed in look at the merged object in (b).

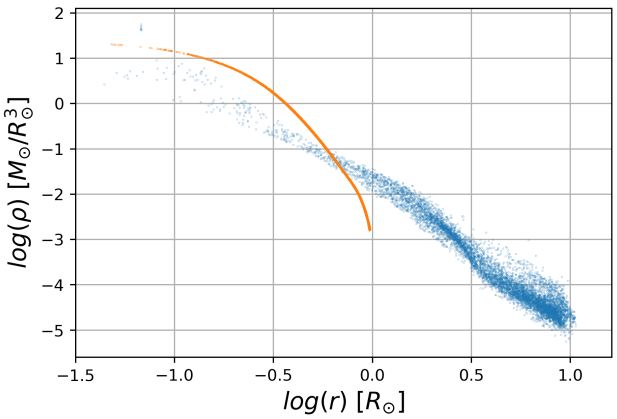


Figure 9: Density of the particles composing the merged object as a function of distance in a direct capture encounter with a WD with $v_{inf} = 1.3$ and $d_{min} = 0.15$. The orange line indicates the original density distribution, while the blue points indicate the density distribution 16.7 dynamical time scales into the simulation.

Figure 8 presents an example of the final state of a direct merger encounter between a WD with $v_{inf} = 1.3$ and $d_{min} = 0.0$ and a MS star. As it can be seen in Figure 8*a* the outer regions of the MS star have been heavily distorted, and there has been a large momentum deposit along the path the WD took to settle in the core of the star. As expected, due to the lower $v_{inf}$ than in the destruction scenario there are fewer unbound particles in Figure 8*b*, and they do not extend as far from the merged object.

Figure 9 displays the density distribution of the MS star before the encounter and of the merged object 16.7 dynamical time scales into the encounter. The region in the very core of the merged object where the density has majorly increased is due to the WD accreting mass along its path in the MS star and now being located there. However, in most of the other parts of the star the density has heavily decreased, except a slight increase in the envelope region of the original MS star. Similarly as in the case depicted in Figure 4 a large momentum deposit took place in the core of the MS star. Hence, the particles in the inner parts of the star gained large momentum, and through number of collisions spread this momentum through outer parts of the star. Leading to an envelope extending up to 10 $R_{\odot}$. The reason the envelope in this type of encounter extends further than in the destruction encounter in Figure 4 is because the momentum gained by the envelope particles is smaller, meaning they do not gain the necessary velocity to escape the gravity of the merged object.

How the mass of the bodies in the system changed during the time of the simulation can be seen in Figure 10. A characteristic of direct merger cases is a very sharp accretion of mass by the WD. Initially the mass change of the WD and the MS star is approximately linear. As soon as the WD has became heavier than the MS star it becomes the main gravitational body in the system, and over a single simulation step has accreted the remainder of the MS stars mass. After the merging has taken place, the system stabilizes in an equilibrium over time, with the merged object containing approximately 1.4 $M_{\odot}$. This involves some of the particles which originally composed the envelope of the MS star to be gravitationally stripped from the merged object by unbound particles. Due to the inherited momentum from the shock wave induced by the WD during the encounter, the unbound particles have positive net momentum away from the merged object. Despite this, it is possible that some of them remain bound to the merged object by losing energy through mutual collisions, and merge with the merged object through lengthy orbits.

The fact that the illustrated case is a direct merger is further supported by investigating the specific orbital energy $\epsilon$ change during the encounter, which can be seen in Figure 11. A large decrease in the specific orbital energy occurs when the WD collides with the MS star, depositing a fraction of its kinetic energy into the star. During the following simulation steps the WD accretes mass from the MS star and shortly after the merger takes place. Once the merger has taken place, as suggested by the mass distribution Figure 10, only the WD remains. This implies that the specific orbital energy is undefined, and for convince of illustration I have set the value in this case to be displayed as zero. The small dips in energy after the merger has taken place are due to the analysis code identifying a couple of very closely situated particles as the MS star.

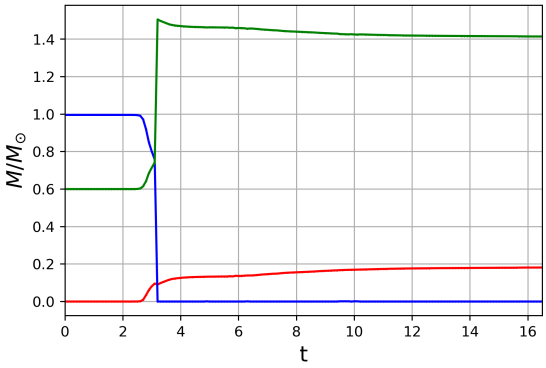


Figure 10: Mass as a function of time in an encounter with WD with $v_{inf} = 1.3$ and $d_{min} = 0.15$, where the WD directly merges with the MS star. Blue line displays the mass of the MS star, green that of the WD, and red the unbound mass.

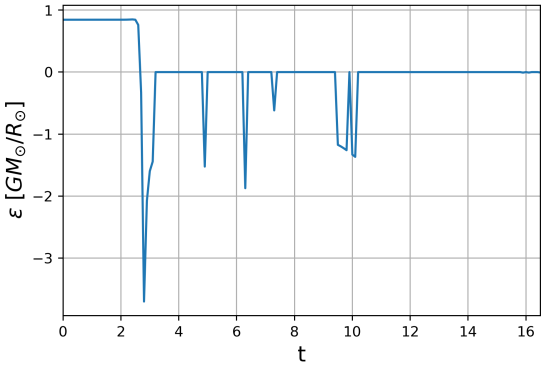


Figure 11: Specific orbital energy $\epsilon$ of the system during a direct merger encounter with WD with $v_{inf} = 1.3$ and $d_{min} = 0.15$ as a function of dynamical time scales.

### 3.1.3 Capture during orbits of the WD

Capture during orbits of the WD occurs when the WD maintains enough kinetic energy after the initial collision with the MS star to pass through it or has a periastron value larger than the radius of the MS star, $d_{min} \geq 1.0\ R_{\odot}$, but not enough to escape the gravitational pull. As a result, the WD is captured in orbit around the MS star, the length of which will wary depending on the specific orbital energy $\epsilon$ and how much mass has the WD accreted during its initial passage through or by the MS star. This type of encounter is observed for all of the possible range of periastron values lying in range of the Roche lobe, region around the star where anything in orbit is bound to it, of the MS star, and for sufficiently large $v_{inf}$ values to either carry the WD through the star or not directly fall into it, but not large enough to destroy it or escape the potential well of the MS star.

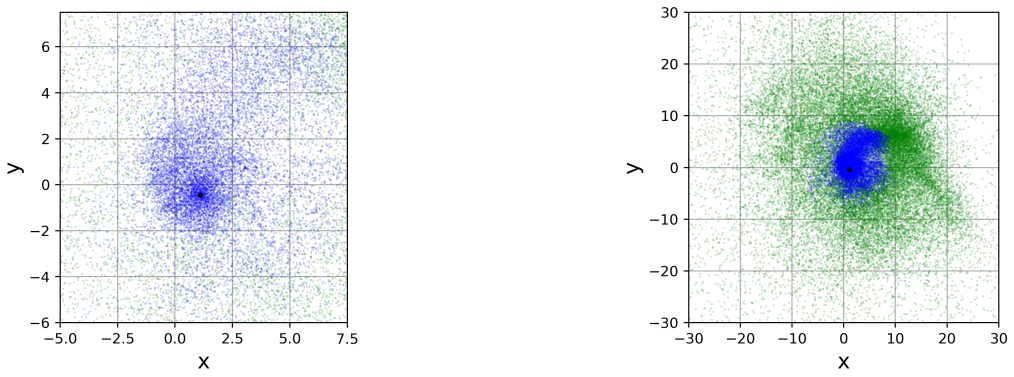


(a) (b)

Figure 12: Illustrations of the merged object resulting from an encounter between MS star and a WD with $v_{inf} = 0.33$ and periastron $d_{min} = 0.4$ undergoing orbital motion around the MS star before merger. Snapshot taken 20.7 dynamical time scales into the simulation. The blue dots indicate the particles composing the merged object, and green are unbound. (a) displays zoomed in look at the merged object in (b).

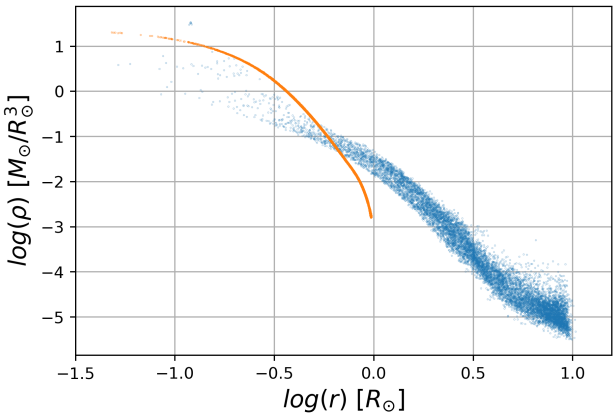


Figure 13: Density of the particles composing the merged object as a function of distance in a orbital capture encounter with a WD with $v_{inf} = 0.33$ and $d_{min} = 0.4$. The orange line indicates the original density distribution, while the blue points indicate the density distribution 20.7 dynamical time scales into the simulation.

Figure 12 displays a scenario in which the WD with $v_{inf} = 0.33$ and $d_{min} = 0.4$ merges with the MS star during the second orbit of the WD. The figure displays the encounter 20.7 dynamical time scales into the simulation, where the WD has already merged with the MS star and settled in its core. Different from the direct capture case in Figure 8, a prominent remnant of the tidal tail trailing in the path of the orbit of the WD can be seen. Just like in direct merger case the unbound particles mainly consist of the envelope of the former MS star, and have captured some of the lesser bound particles from the merged object. Same as in previous cases the inner regions of the merged object have been heavily distorted, which

can be visually seen in Figure 12*a*. One might expect that the total mass of unbound particles in this case will be smaller due to lower $v_{inf}$ and larger $d_{min}$ values. However, that is not true, as, for example, in this particular encounter the WD passed through the MS star two times depositing kinetic energy from two different angles.

As one would expect the density distribution of the merged object strongly resembles the direct capture case in Figure 9, but at the same time also has higher resemblance to the original density distribution. In this particular encounter the envelope does not extend further than in the direct merger in Figure 9 due to the lower $v_{inf}$ value, but interestingly to the same distance at approximately the same density, that is, 10 $R_{\odot}$. The similarities can be attributed to the fact that the WD had multiple collisions with the MS star, and during its orbital motion deposited energy in the envelope particles in a more even spread as can be seen in Figure 12*b*. On top this, the initial collision took place further from the core of the MS star, allowing the WD to deposit its kinetic energy directly in the lighter envelope particles, and the lower velocity allowed for a longer interaction time between the two stars. The core of the merged object has the same point of increased density where the WD resides, lower density in all other regions of the core, and increase in density from approximately 0.5 $R_{\odot}$ when compared to the original distribution.

A hint that the capture has happened during second orbit for this particular encounter can be seen in Figure 14. At approximately 4.0 dynamical time scales into the simulation the WD accretes a noticeable amount of mass from the MS star, some of which is stripped from it by the MS star during subsequent time steps. At around 8.5 dynamical time scales into the simulation a scenario like in the direct merger case takes place, where gradually the WD accretes more mass than the MS star, and the remnant of the MS star becomes bound to the WD. Some of this accreted mass becomes unbound over time, and the total mass of the merged object converges towards 1.4 $M_{\odot}$. Despite this, it can not be said for certain that the merger took place during the second orbit of the WD from Figure 14 alone, as for other $v_{inf}$ and $d_{min}$ values the WD might not accrete any noticeable amount of mass during its first or even second orbit. This would usually happen for larger $d_{min}$ and $v_{inf}$ values that in presented encounter, and the WD would be set on orbits with long orbital period $T$, length of which can be determined using Kepler's third law.

A clear indication that the merger took place during the second orbit of the WD can be seen in the specific orbital energy $\epsilon$ change over time in Figure 15. As the WD collides with the MS star the specific orbital energy drops below 0. While inside the MS star the specific orbital energy is not a good indicator to whether the WD is indeed bound to the MS star as by definition it is not designed to describe such states of the system. However, as can be seen in Figure 15 the orbital energy remains below 0 for an extended period of time after the initial collision, indicating that the WD is in fact bound to the MS star. A large dip in orbital energy can be seen at approximately 8.5 dynamical time scales, which coincides with the merger between the two stars taking place in Figure 14. Once there is only a single body remaining in the system, the specific orbital energy is displayed as 0, a value set of illustration purposes as mathematically it is undefined. The reason that Figure 15 indicates the fact that the merger took place during the second orbit of the WD beyond any doubt, rather than Figure 14, is that exactly two dips in the specific orbital energy can be seen pre-merger and there is an extended period of time between them. Such dips in orbital energy will be present even in encounters where the WD does not accrete any noticeable amount of mass during its

initial orbits around the MS star. On top of this, the value of orbital energy directly shows if the WD is bound to the MS star after the initial orbit.

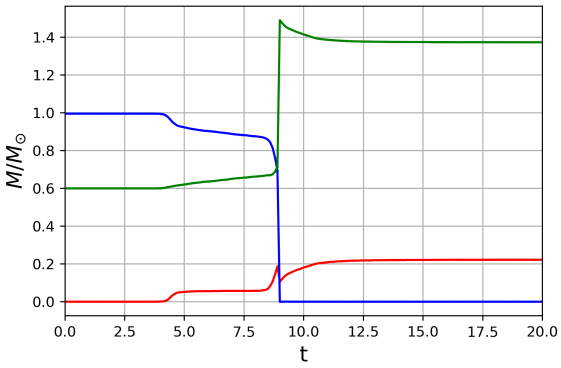


Figure 14: Mass of the bodies in the system as a function of the simulation time in dynamical time scales of an encounter resulting in a merger between the WD and the MS star during second orbit of the WD. Red line represents the total mass of unbound particles, blue the mass of the MS star, and green the total mass of the WD.

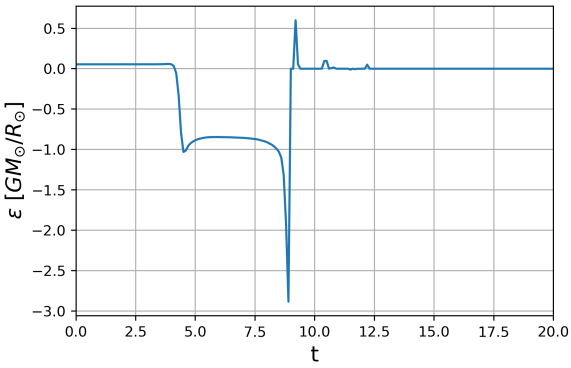


Figure 15: Specific orbital energy as a function of dynamical time scales of an encounter resulting in a merger between a WD and a MS star during the second orbit of the WD.

### 3.1.4 No capture

WD does not get captured when it maintains large enough kinetic energy to escape the gravitational potential of the MS star after the initial encounter with the MS star. This type of encounter can be observed for all possible $v_{inf}$ and $d_{min}$ values. However, the specific range of $v_{inf}$ values depends on the periastron value. As during a physical collision with the MS star $v_{inf}$ must be large enough for the WD to pass through the MS star, while for large periastron values $v_{inf}$ can be smaller. The destruction of MS star encounter type is an extreme velocity sub-category of the no capture encounter.

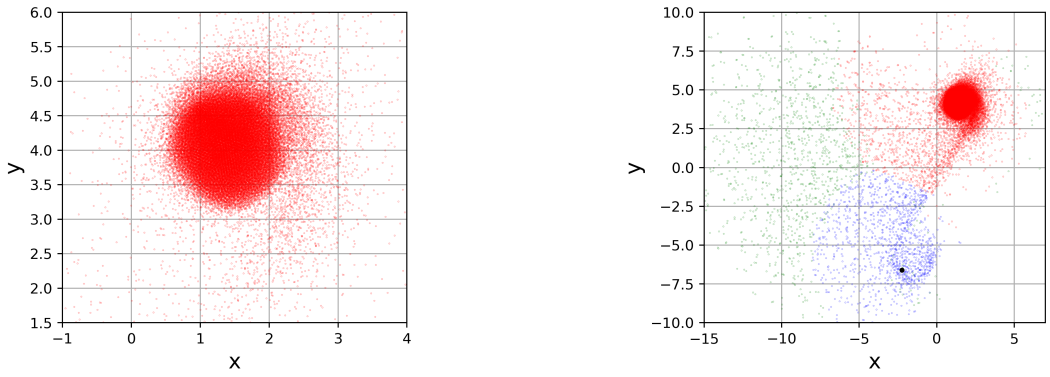


(a) (b)

Figure 16: Illustrations of the system in an encounter between MS star and a WD with $v_{inf} = 0.75$ and periastron $d_{min} = 1.25$ resulting in the WD escaping the potential of the MS star. Snapshot taken 15.1 dynamical time scales into the simulation. The red dots indicate the particles composing the star, green are unbound, and blue accreted by the WD. (a) displays zoomed in look at the MS star in (b).

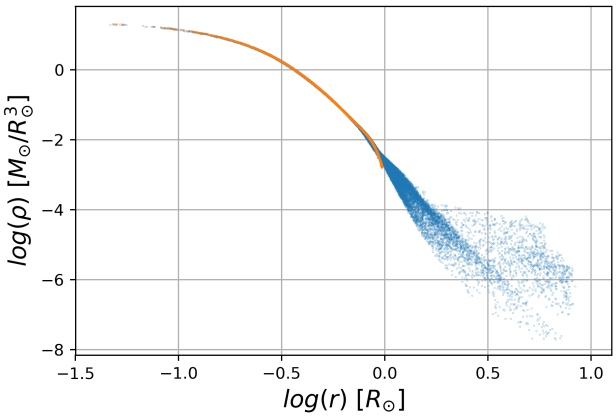


Figure 17: Density of the particles composing the disturbed MS star as a function of distance in a no-merger encounter with a WD with $v_{inf} = 0.75$ and $d_{min} = 1.25$. The orange line indicates the original density distribution, while the blue points indicate the density distribution 15.1 dynamical time scales into the simulation.

An encounter where the WD with $v_{inf} = 0.75$ and $d_{min} = 1.25$ passes through the envelope of the MS star and escapes its gravitational potential can be seen in Figure 16. It can immediately be seen that the the MS star remained relatively unaffected when compared to the previously discussed encounters when comparing Figure 16*a* to other encounter types. All of the distorted particles are those of the envelope, and a weak tidal tail remaining in the path of the WD can be seen in Figure 16*b*. Overall the spherical shape of the MS star has been retained, and as expected this specific encounter has had the least effect on the structure of the MS star of all the presented encounter, especially in this particular encounter as there

was no physical collision between the WD and MS star. Hence, the amount of unbound particles also is the least in this type of encounter.

The structure of the MS star after the encounter remained very similar to the original. In Figure 17 one can see that the inner parts of the star almost did not experience the presence of the WD at all. The only major change can be noticed in the envelope regions, which have been stretched to about 8 $R_{\odot}$, but the overall population and average dislocation of the distorted particles is the smallest of all the encounter types.

No significant change in total mass distribution can be noted in Figure 18. It can visually be seen that the WD accreted some particles in Figure 16*b* and that some were set unbound, but from Figure 18 it can be safely be assumed that these were very low mass envelope particles. Therefore, for purpose of simplicity, it can be assumed that there was no change in mass distribution. The specific orbital energy $\epsilon$ on the other hand did decrease during the passage of the WD, but the change in energy is the smallest of all encounter types. As can be noted from Figure 19 the value of the specific orbital energy never dipped below 0 indicating that the WD is not bound to the MS star.

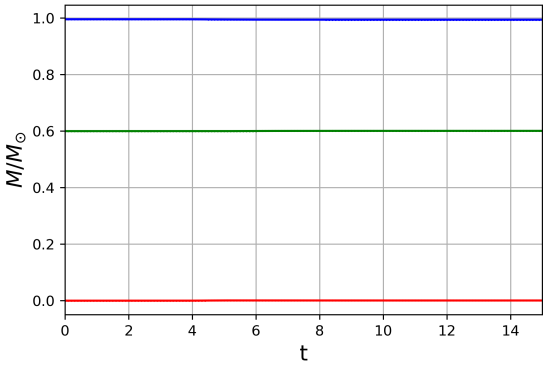


Figure 18: Mass of the bodies in the system as a function of time steps of the simulation of an encounter resulting in the WD remaining unbound. Red line represents the total mass of unbound particles, blue the mass of the MS star, and green the total mass of the WD.

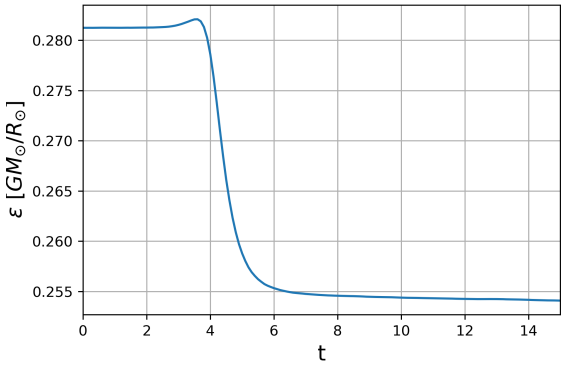


Figure 19: Specific orbital energy as a function of dynamical time scales of an encounter resulting in the WD escaping the gravitational potential of the MS star.

## 3.2 Grid of runs

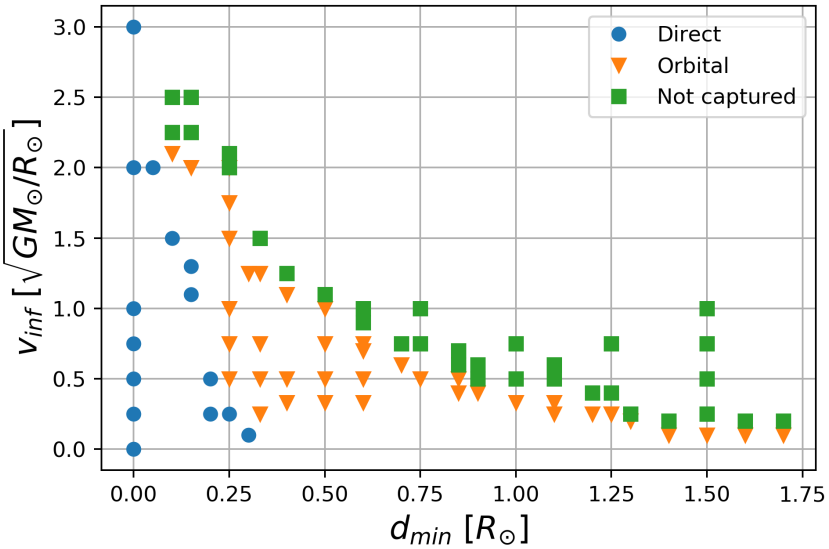


Figure 20: Figure displaying all of the simulated encounters and categorizing the grid of runs based on the outcome of the encounter. Blue points indicate direct merger encounters, orange triangles mergers during orbital motion of the WD, and green squares encounters where the WD escapes the potential of the MS star.

Figure 20 displays all of the encounters performed along side the final result of the encounter. The populating of the figure began by randomly preforming encounters and studying the final specific orbital energy in the no-merger encounters. Depending on how large this value was, the $v_{inf}$ value of the WD was lowered accordingly, while keeping the same $d_{min}$ value. Subsequent encounters with different $v_{inf}$ values were performed until the range of $v_{inf}$ between merger and no-merger encounters was no larger than 0.25 $\sqrt{GM_\odot/R_\odot}$ for $d_{min} \leq 0.5\ R_\odot$, and 0.15 $\sqrt{GM_\odot/R_\odot}$ for $d_{min} > 0.5\ R_\odot$. This procedure was repeated for all of the displayed $d_{min}$ values. As it can be seen there is a strong relation between the outcome and the velocity at infinity $v_{inf}$ and periastron $d_{min}$ values of the WD. The region of particular interest is the boundary between the merger through orbital motion of the WD and no-merger cases as this result provides an insight for the expected impact of WD-MS encounters on the overall stellar population of NSC, depending on the velocity dispersion used in such investigations.

As can be seen in Figure 20 the boundary decreases approximately parabolically for $d_{min}$ values between 0 and 0.25 $R_\odot$, which can be attributed to the decrease in the length of the WDs path through the MS star combined with a rapid decrease in the mass of the particles as the distance from the centre of the star increases. This is followed by a first set of almost linear boundary for $d_{min}$ from 0.25 $R_\odot$ to 0.8 $R_\odot$ which can be attributed to the aforementioned reasons plus the velocity of the WD has became sufficient for it to have prolonged interaction time with the MS star to accrete mass from it. A second linear relation is in the envelope regions of the MS star, that is, for $d_{min}$ values between 0.8 and 1.0 $R_\odot$, where the distance the WD travels through the MS star increases faster with increasing $d_{min}$ value. It is quite

possible that these two linear relations could be connected, but due to lack of resolution it is not possible to tell this from Figure 20. For $d_{min} > 1.0\ R_\odot$ the boundary asymptotically tends towards $v_{inf} = 0$ as $d_{min} \longrightarrow \infty$, which is the expected behaviour given the potential of the MS star decreases as $1/r$.

Note that in Figure 20 the encounter with $v_{inf} = 3.0$, $d_{min} = 0.0$ is categorized as direct merger. However, it lies into a special sub-category not discussed in the section before, where features of destruction and orbital merger are combined. That is, the WD pierces through the MS star heavily distorting the particles composing it, but merges with the remnant of it over a longer time scale than typically observed in direct merger encounters and the WD exits the remnants of the MS star before falling back into them.

The boundary between direct merger and merger through orbital motion of the WD initially exhibits a similar linear pattern to the inner regions of the boundary between merger through orbital motion and no-merger encounters. Despite this, this boundary comes to an abrupt stop at around $0.2\ R_\odot$ for the same reason that the boundary between merger through orbital motion and no-merger keeps decreasing, i. e., the WD after collisions with fewer and lower mass particles maintains enough kinetic energy to pass through the MS star. Further only encounters with very small $v_{inf}$ values exhibit properties of direct merger encounter type.

Despite Figure 20 providing a good overview for ranges of $d_{min}$ and $v_{inf}$ values where one can expected a merger between the stars, lack of resolution of the found boundary has to be noted. For small $d_{min}$ values this should not have a huge impact, as the boundary between merger and no-merger cases lies at very high $v_{inf}$ values, not encountered in most velocity dispersions used in NSC research to date, and the probability of an encounter taking place with small $d_{min}$ according to the collision rate

$$\Gamma(v) = \Sigma n v_{inf} \delta t,\ \Sigma = \pi d_{min}^2 \left(1 + \frac{2GM_\odot}{d_{min} v_{inf}^2}\right), \tag{12}$$

is small (Binney & Tremaine 2008). Equation 12 also indicates that more attention should be paid to encounters with smaller $v_{inf}$ and larger $d_{min}$ values. One could attempt to extrapolate the accurate location of this boundary in Figure 20 in $v_{inf}$ for different $d_{min}$ values using the final value of the specific orbital energy $\epsilon$ from the no-merger case or through study of the orbital period $T$ of the WD in the merger case, discussed later in this section, but due to time constraints this was not carried out.

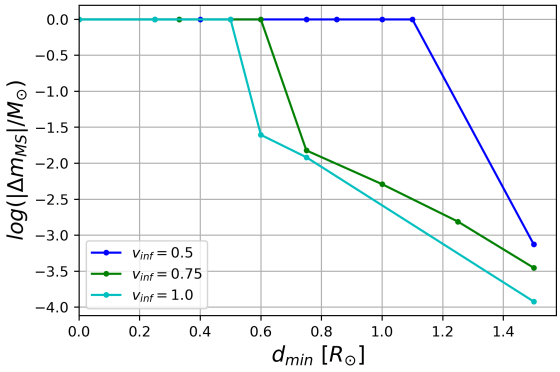


Figure 21: Modulus of the change in total mass of the MS during a set of select encounters performed with different $v_{inf}$ and $d_{min}$ values. The dark blue line displays encounters with $v_{inf} = 0.5$, the green with $v_{inf} = 0.75$, and the cyan with $v_{inf} = 1.0$. For merger encounters it was set that the WD accretes all of the mass of the MS star.

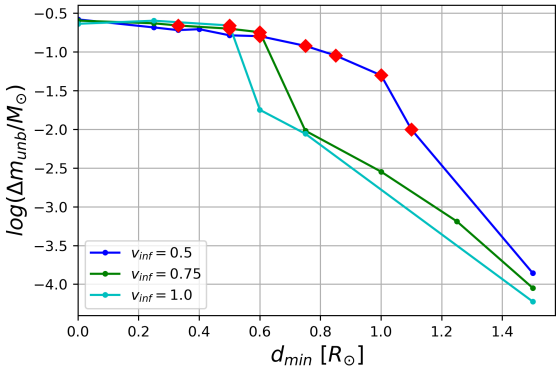


Figure 22: Change in total mass of the unbound matter during a select set of encounters performed with different $v_{inf}$ and $d_{min}$ values. The dark blue line displays encounters with $v_{inf} = 0.5$, the green with $v_{inf} = 0.75$, and the cyan with $v_{inf} = 1.0$. Red diamonds mark extrapolated results for merger encounters with lengthy orbital motion.

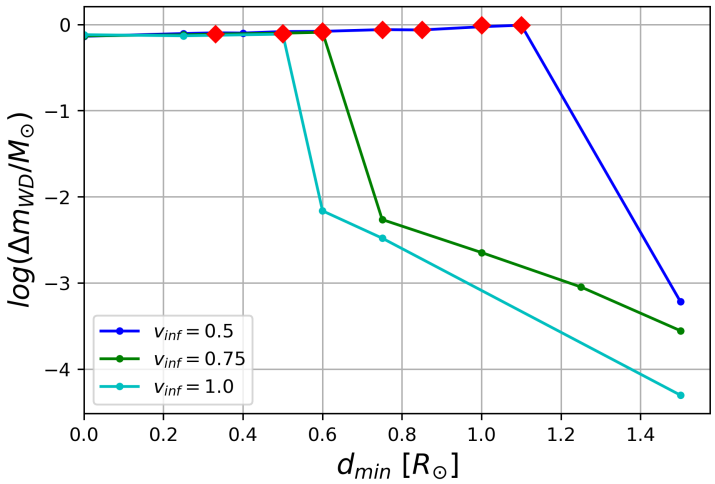


Figure 23: Change in total mass of the WD during select sets of encounters performed with different $v_{inf}$ and $d_{min}$ values. The dark blue line displays encounters with $v_{inf} = 0.5$, the green with $v_{inf} = 0.75$, and the cyan with $v_{inf} = 1.0$. Red diamonds mark extrapolated results for merger encounters with lengthy orbital motion. For merger encounters it was set that the WD accretes all of the mass of the MS star.

Figures 21, 22 and 23 display the difference between final and initial mass of the MS star, unbound mass and the WD in a log scale for different encounters performed with $v_{inf} = 0.5,\ 0.75,\ 1.0$. For illustration purposes, when a merger took place, all of the MS

stars mass was set to be accreted by the WD. This was done in order to display the mass accreted by the WD during no-merger encounters on the same graph. And red diamonds mark extrapolated results for very lengthy orbital merger encounters. The extrapolation was carried out by assuming constant rate of unbound mass increase with increasing periastron value. Figure 22 shows that during merger encounters the amount of generated unbound mass is higher than in no-merger encounters, which is assisted by the fact that the depicted merger encounters had low $d_{min}$ values. For merger encounters, there is more unbound mass generated for larger $v_{inf}$ values, while for no-merger encounters it is the opposite due to the WD having longer interaction time with the MS star when it has lower velocity. In encounters where the WD escapes the gravitational pull of the MS star the mass accreted is very low, even in cases where the WD passes through the MS star, which can be seen in Figure 23. For increasing $d_{min}$ values in no-merger encounters the amount of the mass accreted by the WD, lost by the MS star and set unbound appears to be linearly decreasing in log scale. However, the lack of data points for these encounters for the displayed $v_{inf}$ values prevent me from making any concrete conclusions regarding the further behaviour and further connections between different $v_{inf}$ values. Despite this, one can safely assume that as $d_{min}$ keeps increasing there eventually would be no mass accretion by the WD and no mass loss by the MS star.

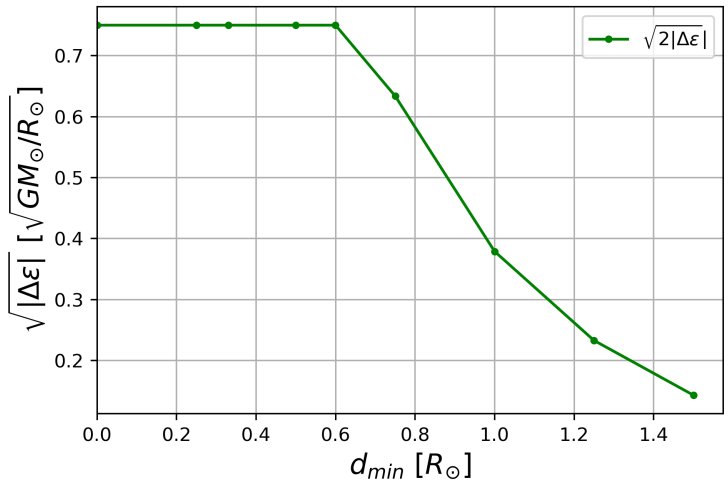


Figure 24: Figure displaying the difference in velocity of the WD between final and initial states of the system of encounters where WD initially has $v_{inf} = 0.75$. For merger encounters the final velocity value was set as $v_{inf} = 0$.

The difference between the final and initial velocity of the WD is displayed in Figure 24. For cases resulting in a merger between the stars, the final velocity was set as 0 $\sqrt{GR_\odot/M_\odot}$. The change in velocity of the WD in Figure 24 is denoted as $\sqrt{2\Delta\epsilon}$, which originates from solving Equation 11 for $|\vec{v}_* - \vec{v}_{PM}|$ as $|\vec{r}_* - \vec{r}_{PM}| \longrightarrow 0$, resulting in $\sqrt{2\epsilon} = |\vec{v}_* - \vec{v}_{PM}|$. Figure 24 suggests that for encounters not resulting in a merger between the stars there is a large kinetic energy loss for the WD, contrary to the possibly expected sling shot effect. For $d_{min} < 1.0\ R_\odot$ this is mostly due the physical collision between the two stars, while for $d_{min} \geq 1.0\ R_\odot$ it is

purely due to mass accretion. The change in $\epsilon$ appears to be asymptotically approaching 0 as $d_{min} \longrightarrow \infty$. While Figure 24 displays the change in velocity only for $v_{inf} = 0.75$, the shape of the graph is almost identical for other $v_{inf}$ values. Examples containing less data points than Figure 24 of cases where $v_{inf} = 0.5$ and $v_{inf} = 1.0$ can be seen in Figure 25. Figure 26 displays the modulus of change of the specific orbital energy $\epsilon$ for all three velocity values on the same axis. As one would expect, for merger encounters the energy change is larger the larger the initial kinetic energy of the WD, while for no-merger encounters the situation is flipped, which can be attributed to the WD accreting more mass from the MS star the lower its velocity, Figure 23. For no-merger encounters the change in $\epsilon$ is linearly decreasing in log scale for increasing $d_{min}$ values.

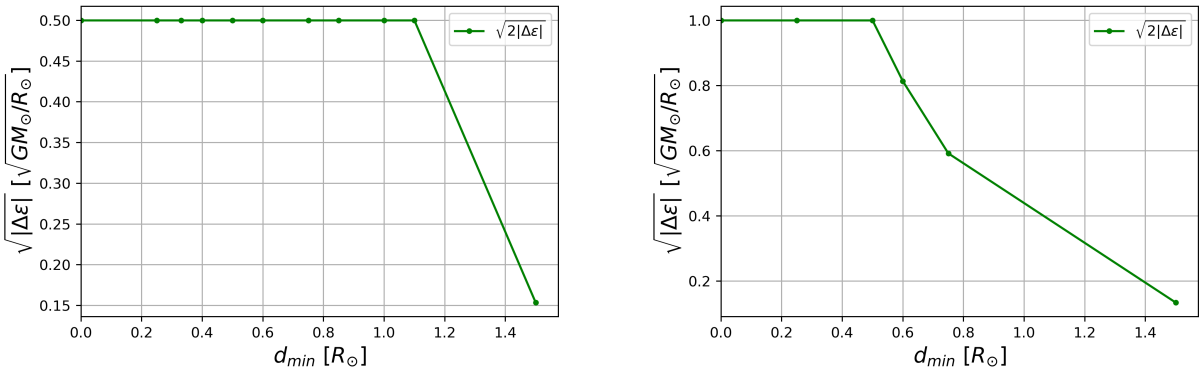


Figure 25: Figure displaying the difference in velocity of the WD between final and initial states of the system of encounters where WD has $v_{inf} = 0.5$ (a) and $v_{inf} = 1.0$ (b). For merger encounters the final velocity value was set as $v_{inf} = 0$.

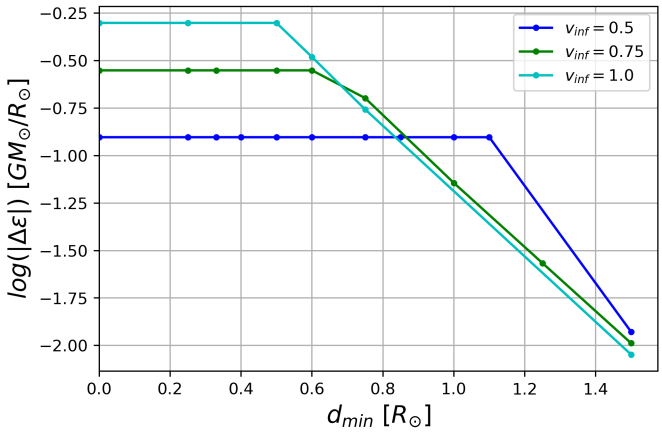


Figure 26: Figure displaying the modulus in difference in specific orbital energy $\epsilon$ between final and initial states of the system for three different WD $v_{inf}$ values. For merger encounters the final energy value was set as $\epsilon = 0$.

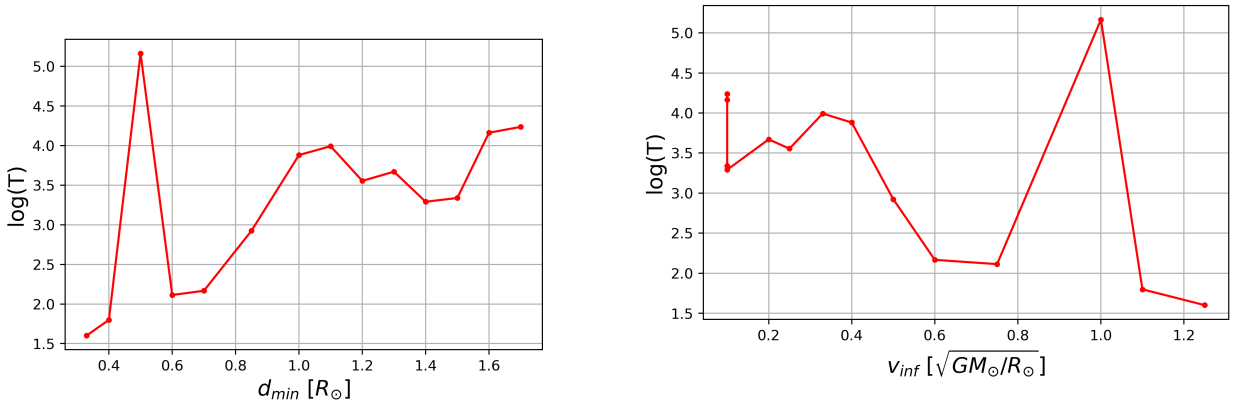


(a) (b)

Figure 27: Figure displaying the orbital period $T$ for encounters at the border between merger and no-merger encounter with respect to periastron value $d_{min}$ (a) and velocity at infinity $v_{inf}$ (b). The orbital period is expressed in dynamical time scales.

Investigation of the orbital period of the encounters located on the border between merger and no-merger in Figure 20 was performed in order to better understand how accurately the boundary has been determined and to put a visualization to how long these periods can be, and how they compare for different $d_{min}$ and $v_{inf}$ values. The obtained results can be seen in Figure 27. As was mentioned, the orbital period $T$ was calculated using using Kepler's third law, and using specific orbital energy $\epsilon$ takes the following form:

$$T = 2\pi\sqrt{\frac{a^3}{GM_{TOT}}} = \frac{\pi GM_{TOT}}{\sqrt{-2\epsilon^3}},\ a = \frac{-GM_{TOT}}{2\epsilon}, \tag{13}$$

where $a$ is the semi-major axis of the orbit, $M_{TOT}$ is the mass of the WD and the MS star after the initial encounter, and $\epsilon$ is also taken after the initial passage of the WD. The period is expressed in dynamical time scales. The expected result was that the orbital period will increase as the velocity decreases and periastron increases, and the obtained results in Figure 27 overall reflect this, apart from a clear outlier at $d_{min} = 0.5$ and $v_{inf} = 1.0$. The reason for this expectation was that, as $d_{min}$ increases and $v_{inf}$ decreases potential and kinetic energy values decrease, making the range of possible change in $\epsilon$ values around the boundary small, paired with the decrease in unbound mass after the initial passage of the WD as $d_{min}$ increases. While the case at $d_{min} = 0.5$, $v_{inf} = 1.0$ might appear as an error, this is not true. In fact, this indicates that the encounter is located perfectly on the boundary between no-merger and merger cases, because the very low energy value indicates that the WD lost just enough kinetic energy to remain bound to the MS star after the encounter. Which in turn implies that other encounters were not as close to the boundary due to the WD still carrying a noticeable amount of kinetic energy. Despite this, one has to recall that period is inversely proportional to the square root of cube of $\epsilon$. Hence, as $\epsilon \longrightarrow 0$ $T$ rapidly increases. Overall Figure 27 does not provide any major insight in the study of encounters between WD and MS stars when considering only single encounter at a time, but can be used as a tool to improve the resolution of the location of the boundary in Figure 20. On top of

this, once the resolution of the boundary has been improved, Figure 27 could be used to estimate the average time it takes for the merger between the stars to take place, and from Equation 13 the semi-major axis $a$ could be used in a similar manner to estimate average orbital distance of the WD and to hypothesize if this could have any impact on frequency of different encounters or the evolution of the stellar population in the NSCs.

# 4 Interpretation

The obtained results indicate that the assumption of no mass loss during merger encounters between MS star and WD made by Mastrobuono-Battisti et al. (2021) was not correct. As it can be seen in Figures 8, 12 and 22 there is a non-negligible amount of unbound mass after the encounters, which over time and number of such encounters taking place in NSC will build up as well as impact the evolution of the merged object. Non-merger encounters also produce some unbound mass, but for larger periastron values it can be ignored, as it is very minor. However, in these encounters the radius of the MS star is increased until the MS star reaches equilibrium once again, see Figure 16, which in turn increases its probability to undergo another encounter. While the destruction scenario encounters produce a large amount of unbound mass, they are extremely unlikely to take place due to the required velocity and periastron values as per Equation 12. Hence, their effect on the evolution of the stellar population could be overlooked. On top of this, Figure 20 shows that the assumption made about the boundary between a merger and non-merger encounter was wrong. That is, encounters with $d_{min} > 1.0\ R_{\odot}$ can merge, and not all encounters with $d_{min} \leq 1.0\ R_{\odot}$ result in a merger, even for the velocity dispersion used by Mastrobuono-Battisti et al. (2021). Per Equation 12 the former will have a larger impact on the overall population of the NSC, leading to more encounters between MS stars and WDs resulting in mergers. Which in turn will lead to more rapid evolution of the MS stars, resulting in increased population of visible giants.

Despite the obtained results convincingly showing that the implemented assumptions by Mastrobuono-Battisti et al. (2021) were not true, one has to note that all the encounters were performed using the same 0.6 $M_{\odot}$ WD and 1.0 $M_{\odot}$, 1.0 $R_{\odot}$ MS star. For more accurate results and estimation of the full impact on the stellar population of NSC over time, scaling needs to be implemented. Consequences of not acknowledging this were already outlined by Mastrobuono-Battisti et al. (2021), where assuming constant WD mass lead to unphysical results of the MS turnoff age. On top of this, the impact of no-merger encounters on the evolution of the remnant star and possible increase of experiencing another encounter also need to be investigated. While no-merger encounters at high velocities were not thoroughly investigated, one can confidently assume that even for larger periastron values a physical collision with a WD with large kinetic energy will have a heavy impact on the future evolution of the MS star, although possibly quite different from a merger.

# 5 Conclusion and future work

It was showed that the assumption made by Mastrobuono-Battisti et al. (2021) of no mass loss in stellar encounters between MS stars and WD is not true as long as there is a physical collision between the two stars. When there is no physical collision between the stars, the amount of unbound mass is very little and can be neglected, see Figure 22. Along side this, it was showed that the assumption that encounters with periastron values larger than 1.0 $R_\odot$ do not result in merger for any $v_{inf}$ values is not true and that for $d_{min} \leq 1.0\ R_\odot$ not all encounters result in a merger, as suggested by Figure 20. However, as previously discussed, per Equation 12 and the velocity dispersion used by Mastrobuono-Battisti et al. (2021) the former will have a larger impact on NSC population as they are more common.

Possible improvements for the project include, but are not limited to, the following suggestions. Optimization of SPH code by implementing alternating time step and reworking the computational methods to increase the computational time and accuracy of low energy encounters. One of the methods which could be used for this is the so called resolution test, where the number of particles used for the discretization is increased and the newly obtained results compared to the existing ones. Implementing an alternative computational method to SPH is also possible. Besides how the encounters were carried out, there is the fact that all the encounters were investigated using a 0.6 $M_\odot$ WD and 1.0 $M_\odot$, 1.0 $R_\odot$ MS star. Therefore, the obtained result in Figure 20 only accurately describes the outcome of encounters with similar parameters of the WD and MS star. In order to fully understand the boundary between merger and no-merger encounters scaling of both the mass of the WD and the mass and radius of the MS star needs to be implemented. On top of this, the resolution of the boundary between encounter types for certain $v_{inf}$ and $d_{min}$ needs to be improved as suggested by Figure 27. The suggestion of performing extrapolation can be used to refine the boundary between no merger and merger encounters, but due to the use of spherical approximation for the potential term in Equation 11 and the necessary accuracy when distinguishing between a merger and no merger, it is suggested that such result is only used as guidance for future simulations or a boundary range estimation. On top of this, due to how SPH code works, it was not possible to confidently state that the obtained result for limiting cases where $v_{inf} \longrightarrow 0$ and $d_{min}\ \epsilon\ (1.4\ R_\odot; \infty)$ is completely accurate. This is because the criteria used to determine if the WD is bound, that is, $\epsilon < 0$ after the initial passage of the WD implies it being bound. However, as the kinetic energy of the WD is decreased and periastron value increased the uncertainty in $\Delta\epsilon/\epsilon$ in SPH increases, and for sufficiently small values noise dominates. If one desires high accuracy, the spherical potential term in Equation 11 should be replaced with general potential energy expression in integral form at least for high velocity and low periastron encounters, and the computational methods reworked for cases where $v_{inf} \longrightarrow 0$.

While the extrapolated results in Figures 22 and 23 were clearly a merger type encounters, the extrapolated values for unbound mass in Figure 22 appear inaccurate. On top of this, some of the final energy values for no-merger cases can only be regarded to as approximations, as the kinetic energy had not yet fully converged to the final value and would have taken several extra dynamical time scales to do so. Overall the data set presented in Figures 21 to 26 is quite small, and to make concrete conclusions beyond identifying similarities between different input parameters would require it to be more populated.

The destruction of the MS star encounters require further investigation. The analysis code interprets the MS star as a bound object, which is contrary to the expected result, but for the particular encounter presence of bound particles can be explained. I see no use in attempting the encounter with even higher $v_{inf}$ value as $v_{inf} = 5.0$ is already extremely unlikely to ever be observed, especially when combined with periastron value of $d_{min} = 0\ R_{\odot}$, but the option that all of MS stars mass is set unbound for even higher $v_{inf}$ value can not be ruled out. In addition, the SPH code is unable to simulate the future evolution of this remnant object. Hence, no conclusive argument can be made on the full impact of this encounter on the MS star apart from heavy distortion of its matter, as can be seen in Figure 3. Similarly, the evolution of other types of encounter should be investigated. While we have overall knowledge of the effects of merger encounters on the future evolution of the merged object, a distinction between merger type of encounters can be made, and the degree of impact on the MS star of encounters not resulting in a merger similarly will wary depending on the WDs $v_{inf}$ and $d_{min}$ values. The hypothesized increase in probability of a subsequent encounter taking place in no-merger encounters where the radius of the MS star is enlarged also needs to be investigated, which would involve investigating the time it takes for the MS star to return to equilibrium configuration, the probability of such encounter occurring and the average increase in radius of the MS star in such encounters.

In conclusion, the obtained results showed, the applied assumptions by Mastrobuono-Battisti et al. (2021) were not fully correct. While requiring refinement and having room for many possible improvements, the located boundary between merger and no merger encounters depending on velocity at infinity $v_{inf}$ and periastron $d_{min}$ of the WD between 0.6 $M_{\odot}$ WD and 1.0 $M_{\odot}$ MS star did not agree with the assumption made. Four different encounter types were found and analysed. The distribution of mass in them was investigated, displaying that when a physical collision between the two stars takes place, there is resulting unbound mass. The amount of which can not be overlooked if one in concerned about future evolution of the MS star or the merged object. Other properties between different encounters were also investigated, but none of the obtained results contradicted expectations. On the basis of these results, the impact of stellar encounters on the evolution of stellar population of NSCs should be revised, and assumptions made for other types of stellar encounters should be looked into in case similar contradictions can arise.

# References


Appel, A. W. 1985, SIAM, 6, 85

Barnes, J. & Hut, P. 1986, Springer, 267

Benz, W. 1986, Springer, 320, 269

Binney, J. & Tremaine, S. 2008, Galactic Dynamics: Second Edition (Princeton University Press)

Eggleton, P. P. 1971, MNRAS, 151, 351

Giersz, M., Heggie, D. C., Hurley, J. R., & Hypki, A. 2013, MNRAS, 431, 2184

Gillessen, S., Plewa, P. M., Eisenhauer, F., et al. 2017, APJ, 837, 30

Gingold, R. A. & Monaghan JJ. 1977, MNRAS, 181, 375

Jernigan, J. G. 1985, I.A.U., 113

Mastrobuono-Battisti, A., Church, R. P., & Davies, M. B. 2021, MNRAS, 505, 3314

Monaghan, JJ. & Mattanzio, J. C. 1985, A& A, 149, 135

Pols, O. R., Tout, C. A., Eggleton, P. P., & Han, Z. 1995, MNRAS, 274, 964

Schödel, R., Feldmeier, A., Kunneriath, D., et al. 2014, A&A, 566, A47

Schödel, R., Nogueras-Lara, F., Gallego-Cano, E., et al. 2020, A&A, 641, A102

Wood D. 1981, MNRAS, 194, 201

# 6 Appendix A

```
import numpy as np

#Reading in data.
Number indicates the number of the output file used for original composition

def doAnalysis(idoc,fn,pmfn):
   x_1 =      np.loadtxt(fn, usecols=(0))
   x_pm_1 =   np.loadtxt(pmfn, usecols=(0))
   y_1 =      np.loadtxt(fn, usecols=(1))
   y_pm_1 =   np.loadtxt(pmfn, usecols=(1))
   z_1 =      np.loadtxt(fn, usecols=(2))
   z_pm_1 =   np.loadtxt(pmfn, usecols=(2))
   v_x_1 =    np.loadtxt(fn, usecols=(3))
   v_y_1 =    np.loadtxt(fn, usecols=(4))
   v_z_1 =    np.loadtxt(fn, usecols=(5))
   v_x_pm_1 = np.loadtxt(pmfn, usecols=(3))
   v_y_pm_1 = np.loadtxt(pmfn, usecols=(4))
   v_z_pm_1 = np.loadtxt(pmfn, usecols=(5))
   m_1 =      np.loadtxt(fn, usecols=(8))
   m_pm_1 =   np.loadtxt(pmfn, usecols=(6))

   Npcls = len(x_1)

   #Calculating positions and velocities

   #r_1 = (x_1**2 + y_1**2 + z_1**2)**(1/2)
   #r_pm_1 = (x_pm_1**2 + y_pm_1**2 + z_pm_1**2)**(1/2)
   #v_1 = (v_x_1**2 + v_y_1**2 + v_z_1**2)**(1/2)
   #v_pm_1 = (v_x_pm_1**2 + v_y_pm_1**2 + v_z_pm_1**2)**(1/2)

   #calculating the required energy values
   M_1 = np.sum(m_1)

   # Calculate position of whole star
   product_x_1 = x_1*m_1
   total_x_1 = np.sum(product_x_1)
   position_x_1 = total_x_1/M_1

   product_y_1 = y_1*m_1
   total_y_1 = np.sum(product_y_1)
   position_y_1 = total_y_1/M_1

   product_z_1 = z_1*m_1
```

```
total_z_1 = np.sum(product_z_1)
position_z_1 = total_z_1/M_1

# Calculate velocity of whole star
product_v_x_1 = v_x_1*m_1
total_v_x_1 = np.sum(product_v_x_1)
velocity_x_1 = total_v_x_1/M_1

product_v_y_1 = v_y_1*m_1
total_v_y_1 = np.sum(product_v_y_1)
velocity_y_1 = total_v_y_1/M_1

product_v_z_1 = v_z_1*m_1
total_v_z_1 = np.sum(product_v_z_1)
velocity_z_1 = total_v_z_1/M_1

Xpm0 = np.zeros(3)
Vpm0 = np.zeros(3)
Xpm0[0:3] = (x_pm_1, y_pm_1, z_pm_1)
Vpm0[0:3] = (v_x_pm_1, v_y_pm_1, v_z_pm_1)
mpm0 = float(m_pm_1)

unbound_prev = -1
star_prev = -1
pm_prev = -1


for j in range(100):

   #definining energies and their components, G=1

   KE_i_1 = np.zeros(Npcls)
   KE_pm_1 = np.zeros(Npcls)
   PE_i_1 = np.zeros(Npcls)
   PE_pm_1 = np.zeros(Npcls)

   for i in range(Npcls):
      vstar = np.sqrt((v_x_1[i] - velocity_x_1)**2 +
      (v_y_1[i] - velocity_y_1)**2 + (v_z_1[i] - velocity_z_1)**2)
      xstar = np.sqrt((x_1[i] - position_x_1)**2 +
      (y_1[i] - position_y_1)**2 + (z_1[i] - position_z_1)**2)
      KE_i_1[i] = 1./2.*vstar**2
      PE_i_1[i] = M_1/xstar

      vpm   = np.sqrt((v_x_1[i] - v_x_pm_1)**2 +
```

```
   (v_y_1[i] - v_y_pm_1)**2 + (v_z_1[i] - v_z_pm_1)**2)
   xpm   = np.sqrt((x_1[i] - x_pm_1)**2 +
   (y_1[i] - y_pm_1)**2 + (z_1[i] - z_pm_1)**2)
   KE_pm_1[i] = 1./2.*vpm**2
   PE_pm_1[i] = m_pm_1/xpm

epsilon_i_1 = KE_i_1 - PE_i_1
epsilon_pm_1 = KE_pm_1 - PE_pm_1


#definining lists for counting where particles belong
unbound_1 = 0
star_1 = 0
pm_1 = 0

mstar = 0.
munbound = 0.
mpm = mpm0

Xstar = np.zeros(3)
Vstar = np.zeros(3)

Xpm   = np.zeros(3)
Xpm[0:3] = Xpm0[0:3] * mpm0
Vpm   = np.zeros(3)
Vpm[0:3] = Vpm0[0:3] * mpm0

iobj = [0 for i in range(Npcls)]

#loop counting how many particles belong where

for i in range(Npcls):

   estar = epsilon_i_1[i]
   epm   = epsilon_pm_1[i]

   if M_1>0:

      if estar>0 and epm>0:
         unbound_1 += 1
         munbound += m_1[i]
         iobj[i] = 0

      elif estar < epm:
         star_1 += 1
```

```
            mstar += m_1[i]
            Xstar[0] += x_1[i] * m_1[i]
            Xstar[1] += y_1[i] * m_1[i]
            Xstar[2] += z_1[i] * m_1[i]
            Vstar[0] += v_x_1[i] * m_1[i]
            Vstar[1] += v_y_1[i] * m_1[i]
            Vstar[2] += v_z_1[i] * m_1[i]
            iobj[i] = 1

         else:
            pm_1 += 1
            mpm += m_1[i]
            Xpm[0] += x_1[i] * m_1[i]
            Xpm[1] += y_1[i] * m_1[i]
            Xpm[2] += z_1[i] * m_1[i]
            Vpm[0] += v_x_1[i] * m_1[i]
            Vpm[1] += v_y_1[i] * m_1[i]
            Vpm[2] += v_z_1[i] * m_1[i]
            iobj[i] = 2

      else:
         if epm>0:
            unbound_1 += 1
            munbound += m_1[i]
            iobj[i] = 0

         else:
            pm_1 += 1
            mpm += m_1[i]
            Xpm[0] += x_1[i] * m_1[i]
            Xpm[1] += y_1[i] * m_1[i]
            Xpm[2] += z_1[i] * m_1[i]
            Vpm[0] += v_x_1[i] * m_1[i]
            Vpm[1] += v_y_1[i] * m_1[i]
            Vpm[2] += v_z_1[i] * m_1[i]
            iobj[i] = 2


#printing results
print('Number of unbound particles (in ', idoc, 'th document):', (unbound_1),
'mass', munbound)
print('Number of particles belonging to the star :', (star_1),
'mass', mstar)
print('Number of particles belonging to the PM :', (pm_1),
'mass', mpm)
```

```
#print('Mass of the star:', mstar)
#print('Mass of the PM:', mpm)
#print('Unbound mass:', munbound)

(position_x_1, position_y_1, position_z_1) = Xstar / mstar
(velocity_x_1, velocity_y_1, velocity_z_1) = Vstar / mstar
(x_pm_1, y_pm_1, z_pm_1) = Xpm / mpm
(v_x_pm_1, v_y_pm_1, v_z_pm_1) = Vpm / mpm

vPmStar = np.sqrt((velocity_x_1-v_x_pm_1)**2 + (velocity_y_1-v_y_pm_1)**2
+ (velocity_z_1-v_z_pm_1)**2)
xPmStar = np.sqrt((position_x_1-x_pm_1)**2 + (position_y_1-y_pm_1)**2
+ (position_z_1-z_pm_1)**2)
ePmStar = .5*mstar*mpm/(mstar+mpm)*vPmStar**2 - mstar*mpm/xPmStar
Energy = ePmStar/(mstar*mpm/(mstar+mpm))
print('Specific energy is:', Energy)
print('')
if (ePmStar < 0.):
   print('Point mass is bound to star!')
   print('')

if (unbound_1 == unbound_prev and star_1 == star_prev):
   print("Converged after ", j, " iterations")

   # Write out objects into separate files
   fp0 = open("%s.0"%(fn), "w")
   fp1 = open("%s.1"%(fn), "w")
   fp2 = open("%s.2"%(fn), "w")
   fps = [fp0, fp1, fp2]
   for i in range(Npcls):
      fps[iobj[i]].write("%s %s %s %s %s %s %s\n"%
      (x_1[i], y_1[i], z_1[i], v_x_1[i], v_y_1[i], v_z_1[i], m_1[i]))
   for i in range(3): fps[i].close()

   # Write out properties of binary
   fpout = open("%s.binary.out"%fn, "w")
   fpout.write("%s %s %s %s %s %s %s %s %s %s %s %s %s %s %s %s %s\n"%
   (mstar, mpm, munbound, Energy, position_x_1, position_y_1,
   position_z_1, velocity_x_1, velocity_y_1, velocity_z_1, x_pm_1,
   y_pm_1, z_pm_1, v_x_pm_1, v_y_pm_1, v_z_pm_1))
   fpout.close()
   break
else:
   unbound_prev = unbound_1
   star_prev = star_1
```

```
            pm_prev = pm_1

        M_1 = mstar
        m_pm_1 = mpm



for i in range(11,37):
    for j in range(1,9):
        fn = 'v5b25%0.2d.%.1d.txt'%(i,j)
        pmfn = 'v5b25%0.2d.%.1d.pm.txt'%(i,j)
        doAnalysis("%s.%s"%(i,j),fn,pmfn)
```

# 7 Appendix B

```
import numpy as np
import matplotlib.pyplot as plt

m_star = []
m_pm = []
m_unb = []
energy = []
time = []

def categorize(fn):
    mstar = np.loadtxt(fn, usecols = (0))
    mpm = np.loadtxt(fn, usecols = (1))
    munb = np.loadtxt(fn, usecols = (2))
    eng = np.loadtxt(fn, usecols = (3))
    m_star.append(mstar)
    m_pm.append(mpm)
    m_unb.append(munb)
    energy.append(eng)


for i in range(0,21):
   for j in range(1,9):
      fn = 'v1b15%0.2d.%.1d.txt.binary.out'%(i,j)
      categorize(fn)


for i in range(len(m_star)):
    t = i*0.1
    time.append(t)


for i in range(len(energy)):
   if (np.isnan(energy[i])): energy[i] = 0.



fig1, ax1 = plt.subplots()

ax1.plot(time, m_unb, '-ro', label = r'$m_{unbound}$', markersize = 0.5)
ax1.plot(time, m_star, '-bo', label = r'$m_{star}$', markersize = 0.5)
ax1.plot(time, m_pm, '-go', label = r'$m_{PM}$', markersize = 0.5)

ax1.set_xlabel('t', fontsize = 15)
```

```
ax1.set_ylabel(r'$M/M_{\odot}$', fontsize = 15)
#ax1.set_title(r'$\frac{M_*(t)}{M_{\odot}}$, point mass captured, $v_{inf} = 0.5$, d = 0
ax1.grid()
#ax1.legend()
ax1.set_xlim(left = 0, right = 16.5)

plt.savefig('Mass_change_v13b015', dpi = 350)


fig2, ax2 = plt.subplots()

ax2.plot(time, energy, markersize = 0.5)

ax2.set_xlabel('t', fontsize = 15)
ax2.set_ylabel(r'$\epsilon~[G M_{\odot}/R_{\odot}]$', fontsize = 15)
#ax2.set_title(r'$\epsilon (t)$, $v_{inf} = 0.5, d = 0.25$')
ax2.grid()
ax2.set_xlim(left = 0, right = 16.5)

plt.savefig('Energy_change_v13b015', dpi = 350)


delta_m_star = m_star[-1] - m_star[0]
delta_m_pm = m_pm[-1] - m_pm[0]
delta_m_unb = m_unb[-1] - m_unb[0]
delta_eng = energy[-1] - energy[0]
e_final = energy[-1]

period = np.pi*(m_pm[-1]+m_star[-1])/np.sqrt(-2*energy[-1]**3)

print("Change in mass of the star:", delta_m_star)
print("Change in mass of the pm:", delta_m_pm)
print("Change in the unbound mass:", delta_m_unb)
print("Change in energy:", delta_eng)
print("Period:", period)
```